Influence of availability of calcium on the hydration of tricalcium aluminate (C_3A) in seawater mixed C_3A-gypsum system

Yamei Cai, Dongxing Xuan, Chi Sun Poon*

Department of Civil and Environmental Engineering, The Hong Kong Polytechnic University, Hong Kong

*Corresponding author. Email address: cecspoon@polyu.edu.hk (Chi Sun Poon)

Abstract: This work examined the effects of seawater on the hydration of tricalcium aluminate (C_3A) in C_3A-gypsum and C_3A-gypsum-$Ca(OH)_2$ systems through characterization of hydration heat release, the evolution of aqueous phase composition and hydration products with the hydration time. It was found that seawater increased the dissolution driving force of C_3A and solubility of gypsum, which accelerated the early hydration of C_3A and the formation of ettringite (AFt), leading to a higher hydration degree of C_3A at the early age compared with the deionized water (DI) mixed pastes. After gypsum depletion to form AFt, and in the absence of $Ca(OH)_2$, the formation of chloroaluminate hydrates was slower due to the insufficient Ca resulted in an accumulation of Al in solution. This would delay the subsequent transformation of AFt to monosulphate (SO_4-AFm) and the formation of hydrogarnet (C_3AH_6), which would further reduce the hydration degree of the C_3A at the later ages. However, in the presence of $Ca(OH)_2$, the hydration degree of C_3A-gypsum-$Ca(OH)_2$ at later ages was increased, which was similar to that of the corresponding DI pastes. This can be inferred that the amount of Ca available in seawater mixed cement concrete can affect the hydration degree of C_3A in cement.

Keywords: Seawater; C_3A; Gypsum; Hydration; $Ca(OH)_2$

1. Introduction

Concrete is the most widely used man-made construction material in the world.[1-3] In the last few decades, along with the rapid urbanization, a great number of infrastructural projects have been constructed, especially in developing countries. The global cement production has been thus increasing rapidly from about 1.1 billion metric tons in 1990 to over 4 billion metric tons in 2020.[4, 5] Noticeably, this has also contributed to a growing demand for freshwater which is one of the important constituents in producing cement and concrete products. By 2050, it has been predicted that 75% of the water demand for concrete production will probably emerge in regions that are experiencing water stress.[6] The possible use of seawater for concrete production has consequently gained increasing interest, particularly in remote islands and for the construction of offshore structures. Even though an abundant amount of Cl^- is present in seawater, when the concrete is made with non-metallic reinforcement (i.e., fiber reinforced polymer) [7, 8] or in the case of reinforcement-free concrete, it would not lead to reinforcement corrosion issues that mostly limit the use of seawater in concrete.

It has been reported that seawater can accelerate cement hydration,[9-14] shorten the setting time [11, 15] and decrease the workability.[16-18] These properties of fresh cement paste and concrete are highly related to the aluminate phase in the cement clinkers, i.e., tricalcium aluminate (C_3A).[19, 20] In fact, the hydration of C_3A in cement clinkers could be affected by other phases of cement clinkers. For example, in the case of undersulphated systems, the C_3A reaction occurred before the alite one, thus there was no obvious effect of alite on the C_3A-gypsum reaction [21]. By contrast, in case of properly sulphated systems and in the presence of alite, the formation peak of monosulphate in the hydration process of C_3A was observed to occur earlier because of the adsorption of some SO_4^{2-} by C-S-H gel, but its formation rate was decreased probably due to lesser available space caused by the hydrates of alite [21]. However, to obtain basic knowledge on the main hydration reactions and hydration mechanism, single phase, such

as pure phase of C_3A, is usually explored at first. But research on the influence of seawater on the hydration mechanism of C_3A is still scarce. Our previous study has reported, compared with the rapid hydration of C_3A in C_3A-deionized water (DI) paste, C_3A-seawater (SW) paste presented an induction period.[22] This retardation reasons were summarized as: 1) the co-existence or ion pairing of SO_4^{2-} in seawater and Ca^{2+} poisoned the reactive sites on the surface of C_3A, hindering the dissolution of C_3A. This was presented as the main reason. 2) the precipitation of brucite in the initial hydration on the surface of C_3A can prolong the induction period of C_3A-SW paste for another 30 min. 3) the formation of Friedel's salt in the reaction between Cl^- in seawater and C_3A resulted in an accumulation of Al (element) in the solution due to the deficiency of available Ca^{2+}, which may also impede the dissolution of remaining C_3A. But the actual retardation degree caused by the third reason was not systematically quantified in our previous research, thus this part still needs to be further explored.

In practice, gypsum is always introduced in Portland cement to control the setting time. When gypsum is present, the formation of AFt and the transformation of AFt to AFm are two important reaction stages for the C_3A hydration in cement concrete. But these two reactions are absent in our previous study in both C_3A-SW and C_3A-DI systems. Therefore, to obtain a more comprehensive understanding of the effect of seawater on C_3A hydration present in cement concrete, a certain amount of gypsum should be present in C_3A reaction system. Besides, the portlandite is one of the hydration products of cement owing to the hydration of tricalcium silicate (C_3S) and dicalcium silicate (C_2S).[23-25] Considering that portlandite can provide Ca^{2+} for the reaction of Cl^- and C_3A mentioned above, calcium hydroxide ($Ca(OH)_2$, CH) should be also included in C_3A-gypsum system to further verify the importance of available Ca^{2+} in seawater mixed C_3A-gypsum system.

Thus, in this work, two reaction systems, namely C_3A-gypsum and C_3A-gypsum-CH, were studied. Furthermore, both deionized water (DI) and simulated seawater (SW) were used as the

mixing water in this study. Isothermal calorimetry, inductively coupled plasma/optical emission spectroscopy (ICP-OES), ion chromatography, X-ray diffraction (XRD) were used to monitor the hydration process of C_3A from different perspectives. Additionally, the Gibbs Energy Minimization Software (GEMS) for thermodynamic modelling was applied to simulate the development of the hydrated phases in an equilibrium state for the C_3A-gypsum-DI and C_3A-gypsum-SW system. Also, this GEMS was also used to calculate the saturation index of C_3A in different DI and SW pastes.

2. Materials and experimental methods

2.1. Materials

A same cubic C_3A material was used in this work compared with our previous work, and the specific material information has been given in Ref [22]: the purity of C_3A was higher than 95 %, and its median particle diameter was 13.7 μm. Gypsum (analytical grade) was purchased from UNI-CHEM (Hong Kong) Corporation Limited. Its fineness and morphology are shown in Fig. 1, indicating that the median particle diameter of gypsum with a tabular shape was 22.4 μm.

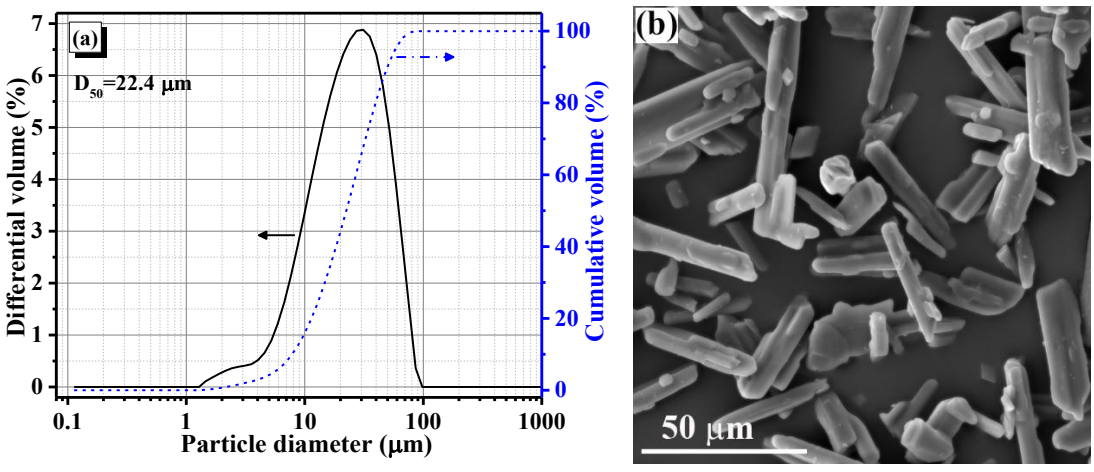

Fig.1. Particle size distribution and morphology of gypsum.

A simulated seawater was prepared according to ASTM D 1141-98.[26] All chemical reagents used in this prepared seawater were analytical grades. The chemical compositions and main ionic concentrations of simulated seawater have been shown in our previous study.[22]

2.2. Sample preparation

2.2.1. Mixing procedures of raw materials

In general, the gypsum content in Portland cements is approximately 30 % to 50 % by mass of the C_3A content.[27, 28] In the reaction system of this study, a gypsum amount of 35 % by mass of C_3A was thus used in the C_3A-gypsum system. To ensure homogeneity, the blended mixture was placed in 50 ml plastic centrifugal tubes, and ethanol was added into these tubes as the mixing medium. These tubes were rotated at 60 rpm for 2 h in an end-over-end rotator. After that, the solid was collected after centrifugation at 10,000 rpm for 5 min, and then placed in a vacuum-drying oven at 40 ^{o}C for 24 h. Afterwards, the dried mixture was gently ground for another 5 min and then stored in a desiccator until use.

For the C_3A-gypsum-$Ca(OH)_2$ (CH) system, the same amount of gypsum was used. Through the stoichiometric calculation, an additional amount of CH accounting for 25 % by mass of C_3A was added to ensure an adequate calcium source in the reaction system. The process of preparation of the homogenous mixture of C_3A-gypsum-CH also followed the steps described above.

2.2.2. Paste preparation

DI and SW were used to prepare C_3A-gypsum or C_3A-gypsum-CH pastes with a water-to-solid ratio (W/S) of 1, and additionally a W/S ratio of 10 was chosen to provide sufficient liquid to measure the evolution of pH value of the reaction systems and to analyse the ionic concentrations. Firstly, according to the stirring procedure described in Ref. [22], the of C_3A-gypsum or C_3A-gypsum-CH pastes was mixed in 50 ml centrifugal tubes. Then, these tubes

were rotated at 40 rpm in an end-over-end rotator to prevent the settlement. At different time intervals from 2 min up to 168 h, solution samples were obtained by centrifugation at 10,000 rpm for 5 min. Pressure filtration was used after 50 h of hydration for the pastes prepared with the W/S ratio of 1. Then, these solution samples/filtrates were filtered through a 0.45 μm membrane filter. About 2.5 mL of filtrates for the C_3A-gypsum paste with a W/S=10 was used to immediately measure the pH value as described in Section 2.3.3. Other filtrates were stored in a fridge at 5 ± 1 °C prior to testing.

In addition, isopropanol was immediately added into the tubes containing the solid residues, and the mass ratio of isopropanol to solid used was about 50:1. After that, these tubes were shaken vigorously to make sure that the solid can be dispersed in the isopropanol as soon as possible. Then a new isopropanol was added to further stop the hydration for 2 d. As for samples at the very early ages, the process of replacing isopropanol can be completed within 5 min. Finally, the samples were dried in a vacuum oven at 40 °C for 1 d. After that, the samples without grinding were placed in a desiccator until further use.

2.3. Testing techniques

2.3.1. Isothermal calorimetry

The development of hydration heat for C_3A-gypsum and C_3A-gypsum-CH pastes mixed with DI or SW was detected at 20 °C using an isothermal calorimeter (Calmetrix, I-CAL 4000). The W/S ratio of 1 was used in this measurement. In order to ensure the homogeneity of pastes, the external mixing method was adopted due to that the very early hydration process was not of interest (< 10 min) [29]. Before testing, all materials used in this test were placed in a temperature-controlled room at 22 ± 1 °C for 24 h. C_3A-gypsum-DI/SW and C_3A-gypsum-CH-DI/SW pastes were mixed for 2 min in calorimetric containers outside the calorimeter, and then these samples were instantly introduced into the calorimeter within 5 min. Meanwhile, the heat release was recorded until the total heat release almost levelled off.

2.3.2. Ionic concentration

The concentrations of anion and cation in the collected filtrates in Section 2.2.2 were monitored using Ion Chromatography (Dionex AS-DV, Thermo Scientific) and inductively coupled plasma/optical emission spectroscopy (ICP-OES, FMX36, SPECTROBLUE). The details of these tests have been described in Ref [22].

2.3.3. pH measurements

The pH of the filtrates collected was measured immediately using a digital display pH meter (PHS-3C) with a precision of 0.01 in order to avoid errors due to carbonation. Before measurement, the commercial buffers at pH of 7.00, 9.21 and 10.01 were used to calibrate the pH meter.

2.3.4. Mineral composition of hydration products

The mineralogy of C_3A-gypsum and C_3A-gypsum-CH pastes was characterized using X-ray diffraction analysis (XRD, Rigaku SmartLab 9kW-Advance). The instrument parameters set in the qualitative test and quantitative test were identical with Ref.[22], other than the scan speed, i.e., 5 °/min for qualitative test and 2.5 °/min for quantitative test in this work.

The quantitative test was used to calculate the hydration degree of C_3A in different hydration time, and an internal standard method was chosen. In the process of Rietveld refinement analysis of XRD pattern, TOPAS software was used. The optimized parameters contained background coefficients, Chebyshev polynomial correction, phase scale factors, zero-shift error, Lorentz polarization factor, cell parameters, adsorption coefficient, peak shape parameters and preferred orientation parameters. A R_{wp} value of below 15 % and GOF value of below 2 correspond to a good Rietveld refinement result. The ICSD codes of the minerals used for the Rietveld refinement analysis are shown in Table 1.

After the Rietveld refinement analysis, the weight fraction of the unreacted C_3A, $W_{C3A,\ Rietveld}$, can be obtained. In order to eliminate the dilution effect of bound water in the hydration products on the Rietveld results, the bound water content was measured by thermogravimetry, and the $W_{C3A,\ Rietveld}$ value was further corrected as $W_{C3A,\ rescaled}$ as described in Ref. [30] After that, the hydration degree of C_3A in different hydration time can be calculated according to the following Equation (2-1).

$$D_{C_3A}=(1-\frac{W_{C_3A,\ rescaled}}{W^0_{C_3A}})\times 100\% \quad (2\text{-}1)$$

Where D_{C_3A} is the hydration degree and $W^0_{C_3A}$ is the weight fraction of initial C_3A in the C_3A-gypsum and C_3A-gypsum-CH pastes before hydration.

Table 1. ICSD codes of the phases used for the Rietveld refinement analysis

Phase	ICSD codes	Reference
Cubic C_3A	1841	[31]
Gypsum	409581	[32]
Ettringite	155395	[33]
AFm-12	100138	[34]
C_3AH_6	94630	[35]
Kuzel's salt	-	[36]
Portlandite	202220	[37]
Corundum	77810	[38]

2.3.5. Thermodynamic analysis

Thermodynamic modelling was carried out to evaluate the evolution of hydration products with time for the C_3A-gypsum pastes using the Gibbs Energy Minimization Software (GEMS),

during which the PSI-Nagra database [39] and Cemdata 18 database [40-42] were used. The specific simulation process has been described in detail by Cai et al.[22]

Based on the measured composition of pore solution of C_3A-gypsum and C_3A-gypsum-CH pastes in the Sections 2.3.2 and 2.3.3, the saturation index of C_3A was calculated using GEMS to evaluate the dissolution driving force of C_3A in different SW and DI water systems. The above two databases were also used in this calculation. The detailed description about saturation index has been given in Ref.[43]

3. Results and discussion

3.1. Influence of seawater on the hydration process of C_3A-gypsum pastes in the absence of calcium hydroxide (CH)

3.1.1. Evolution of hydration heat

Fig. 2 shows the development of heat release of the C_3A-gypsum pastes mixed with DI and SW at a W/S ratio of 1. From Fig. 2 (a), the main exothermic peak of C_3A-gypsum-SW paste appeared at about 15 h earlier than that mixed with DI. However, its main exothermic peak had a lower intensity and smaller slope compared with one mixed with DI. Furthermore, it was observed from Fig. 2 (b) that the increase of the amount of heat release became extremely small after the occurrence of main exothermic peak in the C_3A-gypsum-SW paste. The total heat in the SW paste was about 12 % lower than that in the C_3A-gypsum-DI paste at 96 h, showing lower reaction enthalpies of the SW paste.

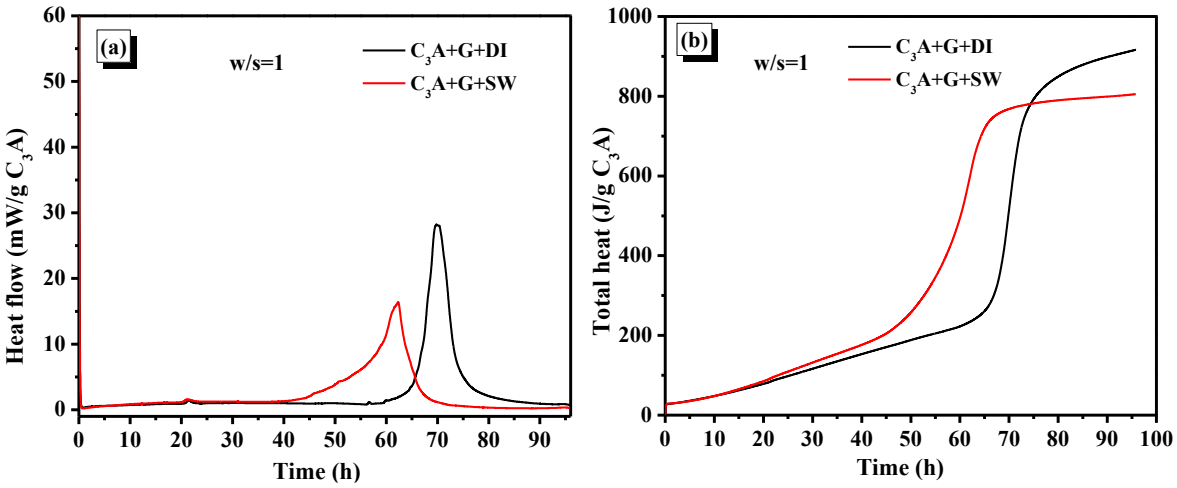

Fig. 2. Evolution of heat flow curves (a) and cumulative heat (b) of C_3A-gypsum-DI/SW pastes with a W/S ratio of 1.

3.1.2. Ionic concentration and pH value

Fig. 3 shows the evolution of ionic concentrations at different reaction times for C_3A-gypsum-DI/SW pastes with a W/S ratio of 1 and 10. Also, the ionic concentrations at time zero denote their initial concentrations in the SW and DI water. The Al, Ca and Mg in the Fig. 3 denote the elements in the pore solutions.

As for the initial dissolution of C_3A, the increase of concentration of Ca (element) for the SW paste was 2 times higher than that of DI paste (Fig. 3 (b)), and there was no accumulation of Al (element) in the solution (Fig. 3 (a)). After about 40 h, there was an increase in the concentration of Al (Fig. 3 (a)) and a depletion of Ca (Fig. 3 (b)) for the SW paste. A same trend can be seen in the paste prepared with a W/S ratio of 10 in Figs. 3 (d) and 3 (e) as well. By contrast, the concentration of Al in the DI paste continued to remain stable at about non-detectable values (Figs. 3 (a) and 3 (d)), and the concentration of Ca also decreased with time, but it was not completely consumed (Figs. 3 (b) and 3 (e)). As for Mg (element) introduced by seawater, its concentration promptly reduced to about non-detectable values at 2 min of

hydration in Fig. 3 (b). The precipitation of Mg in the initial stage of hydration resulted in a decrease of pH value as shown in Fig. 3 (g).

Regarding Cl^- in Fig. 3 (c), its concentration was decreased, which might be mainly due to the formation of Kuzel's salt or Friedel's salt and the adsorption by SO_4-AFm.[44] After 120 h, about 77% Cl^- had been removed, and the concentration of residual Cl^- was 4.3 g/L. A comparable downward trend was seen in the C_3A-gypsum-SW paste prepared with a W/S ratio of 10 in Fig. 3 (f).

As for initial concentration of SO_4^{2-} in the C_3A-gypsum pastes prepared with a W/S of 1 in Fig. 3 (c), compared with an increase shown in the solution of DI paste, there was an initial decrease of SO_4^{2-} concentration in the solution of SW paste. This could be due to the precipitation of gypsum from seawater in the initial stage. This phenomenon has been reported in the tricalcium silicate (C_3S) - seawater paste.[45] Besides, as for the later evolution of SO_4^{2-} concentration in C_3A-gypsum-DI paste with a W/S ratio of 10, its concentration approached to zero before the beginning of the acceleration period of C_3A hydration as reported by previous studies.[46-50] By contrast, SO_4^{2-} was still detectable in the pore solution of the SW paste (Figs. 3 (c) and 3 (f)) before the occurrence of main exothermic peak, and its concentration was still approximately 0.5 g/L at 120 h of hydration for the SW paste prepared with W/S ratios of 1 and 10.

As for the change of pH value in Fig. 3 (g), the pH value in the DI paste slightly increased to 12.47 from 12.38 at 5 min and then marginally decreased to about 12 at 168 h. This was due to the release of OH^- through dissolution of C_3A in the initial hydration and the consumption of OH^- during the precipitation of the hydration products. In comparison, the initial pH value in the SW paste was sharply decreased to about 8.8, which was due to the precipitation of Mg as mentioned above. Then the pH value bounced back to 12.67, which was higher than that in DI paste. This will be further explained in Section 4.4.

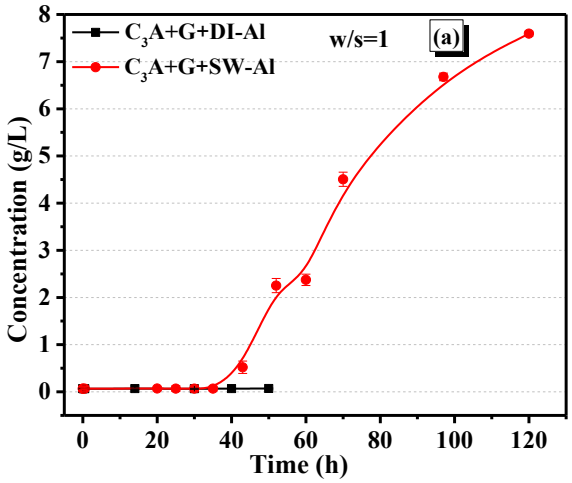
(a)
w/s=1
C3A+G+DI-Al
C3A+G+SW-Al
Concentration (g/L)
Time (h)

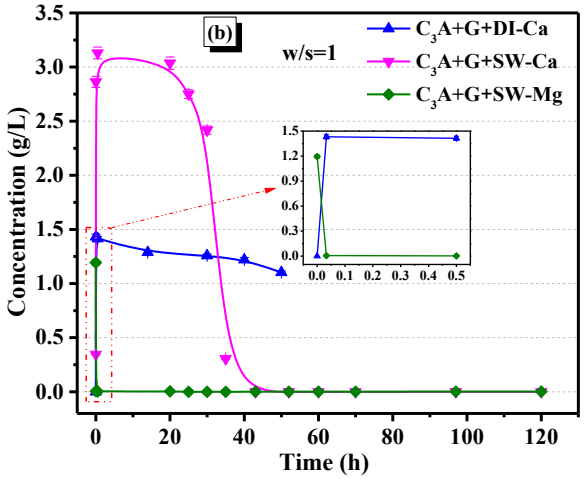
(b)
w/s=1
C3A+G+DI-Ca
C3A+G+SW-Ca
C3A+G+SW-Mg
Concentration (g/L)
Time (h)

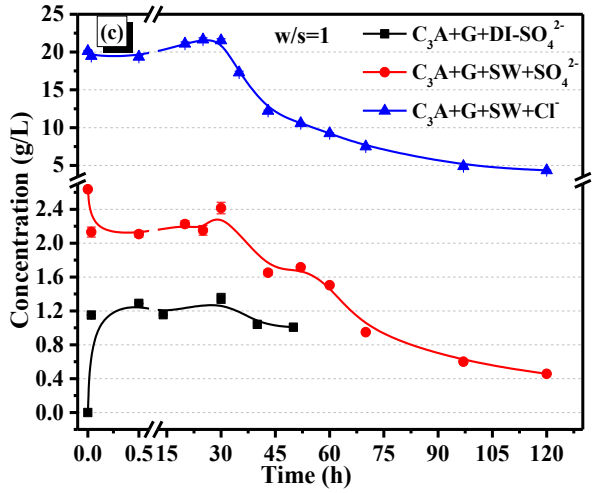
(c)
w/s=1
C3A+G+DI-SO4 2-
C3A+G+SW+SO4 2-
C3A+G+SW+Cl-
Concentration (g/L)
Time (h)

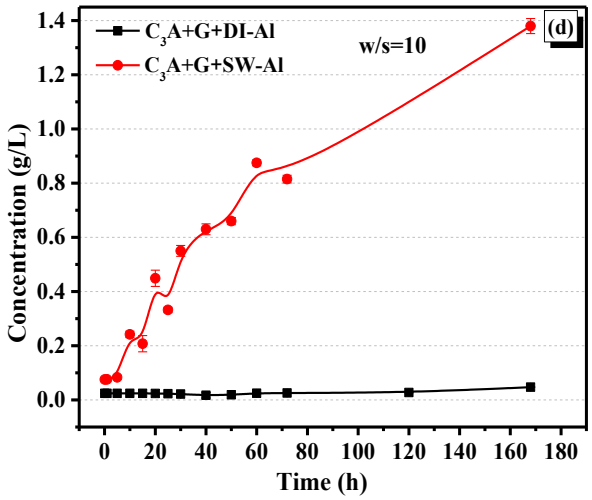
(d)
w/s=10
C3A+G+DI-Al
C3A+G+SW-Al
Concentration (g/L)
Time (h)

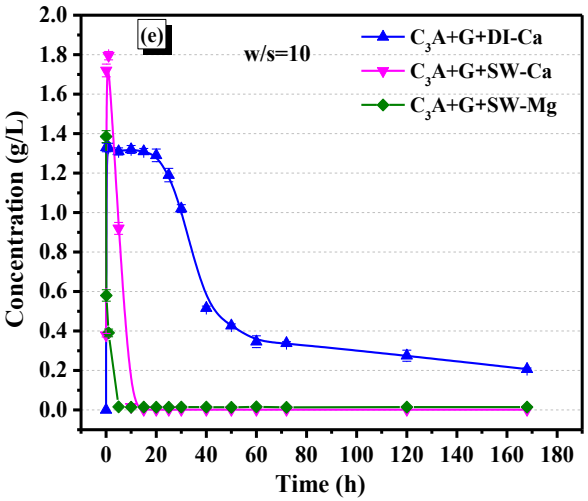
(e)
w/s=10
C3A+G+DI-Ca
C3A+G+SW-Ca
C3A+G+SW-Mg
Concentration (g/L)
Time (h)

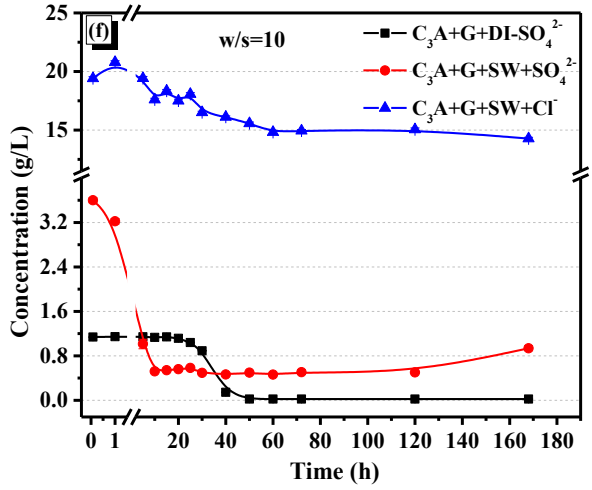
(f)
w/s=10
C3A+G+DI-SO4 2-
C3A+G+SW+SO4 2-
C3A+G+SW+Cl-
Concentration (g/L)
Time (h)

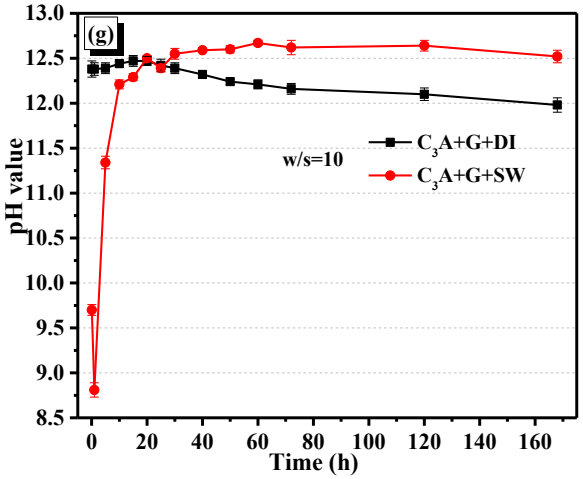

Fig. 3. Change of ionic concentrations and pH value at different reaction times for C_3A-gypsum- DI/SW pastes. (a)-(c) denote the pore solution from pastes with a W/S=1, but it failed to get the solution of the C_3A-gypsum-DI paste after 50 h, even though a pressure of 500 kN was applied. Therefore, the solution centrifuged from pastes with a W/S=10 ((d)-(f)) was mainly to supplement the change of ionic concentrations at later ages.

3.1.3. Evolution of hydration products

Fig. 4 presents the crystalline hydration products at different hydration times for C_3A-gypsum-DI/SW pastes prepared with a W/S ratio of 1. For the DI paste in Fig. 4 (a), the main phases detected were C_3A and gypsum at 30 min, and the hydration product of ettringite (AFt) was found at 30 h. At 50 h, a part of AFt was converted to SO_4-AFm, and then C_3AH_6 was detected from about 60 h onward. After 96 h, almost all C_3A was transformed to SO_4-AFm and C_3AH_6.

By contrast, when seawater was used as the mixing water in Fig. 4 (b), the minerals detected were similar to that in the DI pastes at 30 min and 30 h. However, at 35 h, Kuzel's salt was detected, indicating the presence of the chemical reaction of Cl^- in seawater and C_3A. Then SO_4-AFm was detected at 52 h, but some AFt was still not converted to SO_4-AFm at 52 h and 96 h. Besides, until 192 h, no C_3AH_6 was found in the SW pastes. This represents that the

chemical reaction between Cl^- and C_3A delayed the conversion of AFt to SO_4-AFm and the formation of C_3AH_6. Besides, compared with the DI paste, more unhydrated C_3A was found in the SW paste at 96 h and 192 h, indicating a lower hydration degree at the later ages.

Table 2 illustrates the hydration degree of C_3A in the DI and SW pastes. The results showed that, at 30 min and 30 h, the hydration of C_3A in SW paste was faster than those in the C_3A-gypsum-DI pastes. However, at 96 h and 192 h, the hydration degree of C_3A in SW pastes was about 8 % and 4 % lower than that of the corresponding DI pastes, respectively.

According to the hydration degree of C_3A in SW and DI pastes, the development of mineralogical phases as a function of hydration time was simulated using thermodynamic modelling and the results are shown in Fig. 5. As for the reaction sequence of C_3A-gypsum-DI paste in Fig. 5 (a), AFt was formed first, followed by the conversion of AFt to SO_4-AFm, and the remaining C_3A would be finally hydrated into C_3AH_6. This reaction sequence was consistent with Refs.[28, 47, 51, 52] By contrast, when seawater was used as the mixing water, the first hydration product was AFt, but the formation of AFt was faster than that in the DI paste due to the relatively faster initial hydration degree of C_3A in the SW paste (Table 2). The specific reason for the accelerating formation of AFt in SW system will be further explained in Section 4.3. After that, the Cl^- in seawater would react with C_3A to form a small amount of Friedel's salt at the beginning of reaction. Due to the partial replacement of Cl^- in the Friedel's salt by SO_4^{2-} existed in pore solution, the formed Friedel's salt was quickly converted to Kuzel's salt in this reaction system, but this transition was not captured in Fig. 4 (b). Then, AFt began to transform into SO_4-AFm at a relatively slow rate due to a slower reaction rate of C_3A in the later ages (Table 2). Besides, the C_3AH_6 was not observed in this SW paste.

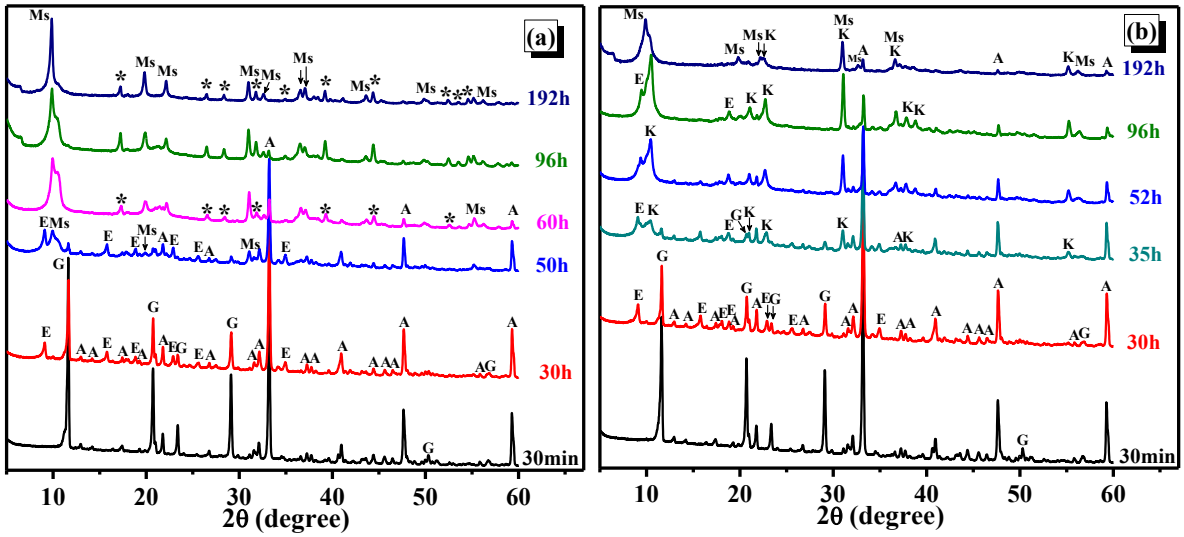

Fig. 4. Hydration products at different reaction times for C_3A-gypsum-DI paste (a) and C_3A-gypsum-SW paste (b) with a W/S ratio of 1. (A: C_3A (tricalcium aluminate), G: gypsum, E: ettringite (AFt), Ms: SO_4-AFm-12, K: Kuzel's salt, ✲: C_3AH_6 (hydrogarnet).)

Table 2. Hydration degree of C_3A in C_3A-gypsum-DI/SW pastes with a W/S ratio of 1 as calculated by QXRD.

Ages	C_3A+G+DI	C_3A+G+SW
30 min	3.6	6.7
30 h	22.8	27.6
96 h	99.5	91.7
192 h	99.5	95.7

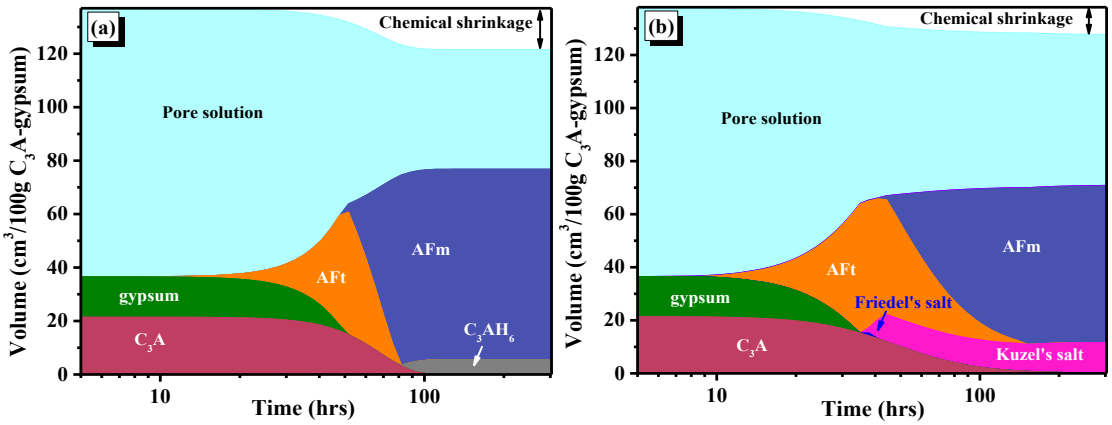

Fig. 5. Modelled development of hydration products at equilibrium in the C_3A-gypsum-DI paste (a) and C_3A-gypsum-SW paste (b).

3.2. Influence of seawater on the hydration process of C_3A-gypsum paste in the presence of calcium hydroxide (CH)

3.2.1. Evolution of hydration heat

Fig. 6 shows the heat evolution rate and the total heat of hydration for the C_3A-gypsum-CH pastes mixed with DI water and seawater. From Fig. 6 (a), when CH was present, there was a relatively longer induction period compared with the pastes without CH in Fig. 2 (a). As reported, this was attributed to 1) the surface deposition of CH on the C_3A particles, 2) the formation of much smaller and thinner ettringite on the C_3A surface in the presence of CH, which can be easier attached on the irregular surface of C_3A.[53-55]

Furthermore, just like that in the C_3A-gypsum-SW paste in Fig. 2 (a), the main peak in this Ca-rich C_3A-gypsum-CH-SW paste in Fig. 6 (a) appeared earlier as well. Even though the intensity and slope of this peak were still lower than the corresponding DI paste, the ascending slope significantly increased compared with that in C_3A-gypsum-SW paste without CH. From Fig. 6 (b), it was also found that the total heat released by C_3A-gypsum-CH-SW paste was lower than that released by DI paste, which was consistent with that in the C_3A-gypsum-SW paste in Fig. 2 (b). This indicates the lower reaction enthalpies in the SW paste.

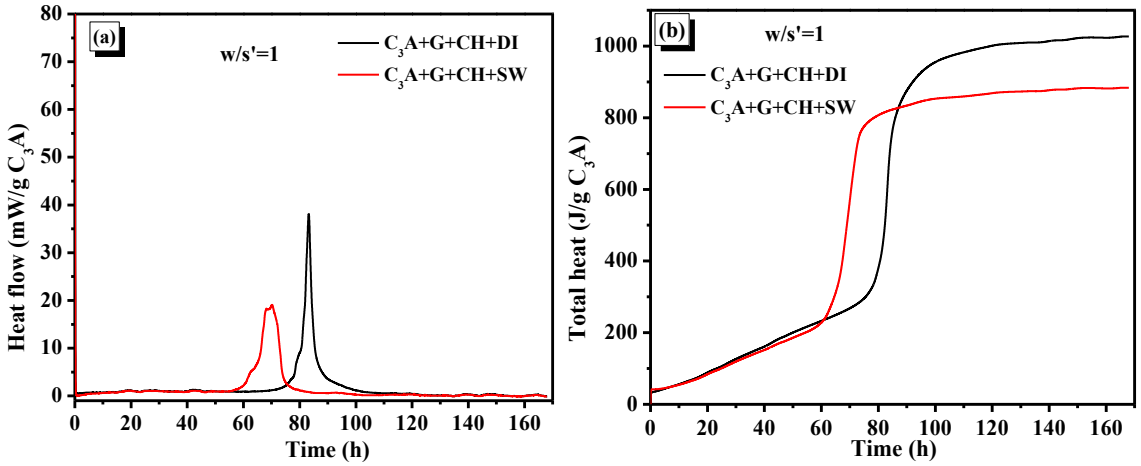

Fig. 6. Development of heat flow (a) and total heat (b) of hydration for C_3A-gypsum-CH-DI/SW pastes. The W/S' denoted the mass ratio of water to the sum of C_3A and gypsum.

3.2.2. Change of concentrations of Ca, Al and Cl^- and pH value

Figs. 7 (a) and 7 (b) display the concentrations of Al (element) and Ca (element) in the pore solution of C_3A-gypsum-CH-DI/SW pastes at different hydration periods. When CH was present in the DI paste, the change of the concentrations of Al and Ca was comparable with those in the C_3A-gypsum-DI paste without CH in Figs. 2 (a), 2 (b), 2 (d) and 2 (e): no Al was accumulated in the solution throughout the reaction process in Fig. 7 (a), and Ca was not depleted in Fig. 7 (b).

By contrast, when CH was added into the SW paste, the concentration of Al in the pore solution always remained very low at both early and later ages, which was different from the result present in the C_3A-gupsum-SW paste in Figs. 2 (a) and 2 (d): an accumulation of higher concentration of Al after the formation of Kuzel's salt and Friedel's salt. This will be further discussed in Section 4.4. As for Ca in Fig. 7 (b), its concentration in the SW paste at 30 h was about 1.8 times higher than that in the DI paste. However, at 70 h and 168 h, there was a relatively lower concentration of Ca in the solution of SW paste, even though the CH was present in this system. This could be due to that the increase of pH value in the SW paste in

Fig. 7 (d) decreased the solubility of Ca. The reason for this pH increase will be explained in Section 4.4.

Fig. 7 (c) compares the concentration of Cl^- in the C_3A-gypsum-SW paste and C_3A-gypsum-CH-SW paste. At 30 h, i.e., before the formation of Friedel's salt and Kuzel's salt, the concentrations of Cl^- in both pastes were similar, showing that the incorporation of CH in C_3A-gypsum-CH-SW paste did not affect the initial concentration of Cl^-. However, the concentration of Cl^- at 70 h of the C_3A-gypsum-CH-SW paste was lower than that in the C_3A-gypsum-SW paste at 70 h and even 120 h. A same phenomenon was also seen at 168 h in the C_3A-gypsum-SW and C_3A-gypsum-CH-SW pastes prepared with a W/S ratio of 10. This indicated that the incorporation of CH accelerated the reaction of Cl^- and C_3A. This could be ascribed to a relatively quicker dissolution rate of C_3A at the later ages due to the lack of Al in the pore solution of C_3A-gypsum-CH-SW paste, as compared to that in the C_3A-gypsum-SW paste. The dissolution driving force of C_3A was further explained in Section 4.2.

Furthermore, as reported in our previous study,[22] when C_3AH_6 began to form in the C_3A-SW paste without gypsum, the concentration of Cl^- in the pore solution fell into the range of 1.3-1.7 g/L. By contrast, it was found that the concentration of residual Cl^- in the C_3A-gypsum-SW paste at 120 h was still 4.3 g/L and its declining rate thereafter was insignificant as shown in Fig. 3 (c). This meant that the reaction of Cl^- and C_3A in the C_3A-gypsum-SW paste was still active after 120 h, which was the reason why C_3AH_6 was not found even at 192 h in Fig. 4 (b).

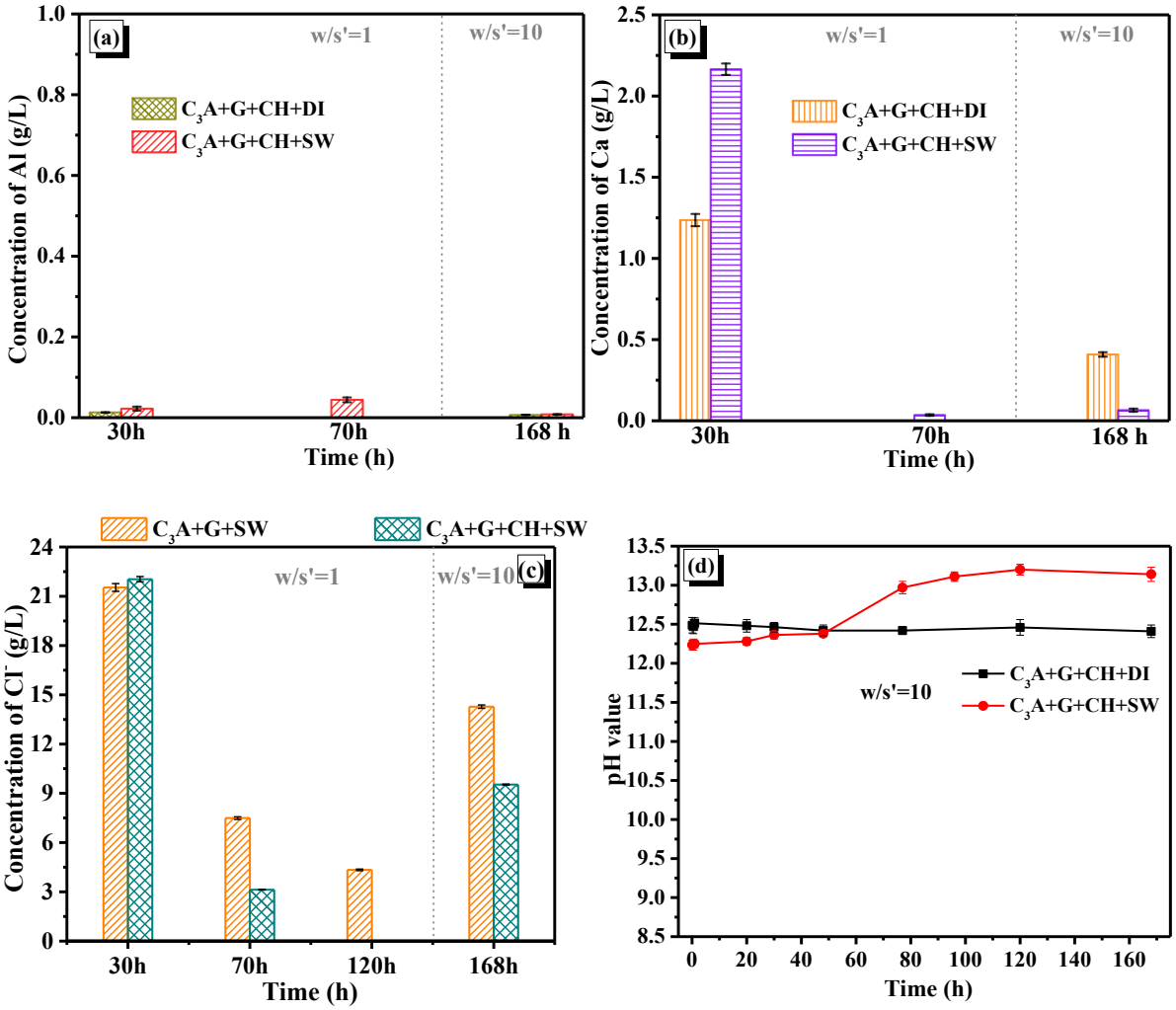

Fig. 7. Change of concentrations of Al (a), Ca (b) and Cl^- (c) and pH value (d) in the pore solution extruded from C_3A-gypsum-CH-DI/SW pastes at different hydration times, and the concentration comparison of Cl^- in both C_3A-gypsum-SW paste and C_3A-gypsum-CH-SW paste (c). (The filtrates at 30, 70 h and 120 h was from pastes with a W/S' of 1, but the pore solution of DI paste at 70 h was not obtained even if a pressure of 500 kN was applied. The filtrate at 168 h was squeezed from pastes with a W/S' of 10 to reveal the change of concentration of Al, Ca and Cl^- at later ages.)

3.2.3. Hydration degree of C_3A in C_3A-gypsum-CH pastes

Table 3 lists the hydration degree of C_3A for C_3A-gypsum-CH-DI/SW pastes prepared with a W/S' ratio of 1. It shows that, at 30 h and 40 h, the hydration degrees of C_3A in the SW pastes

were higher than that in the corresponding DI pastes. This reflects an initial acceleration effect of seawater on the C_3A hydration, which was consistent with the results of C_3A-gypsum-DI/SW pastes in Table 2. The reason for the accelerating reaction between SO_4^{2-} and C_3A in the SW pastes will be further elucidated in Section 4.3. However, at 96 h and 192 h, the hydration degrees of C_3A for the SW pastes were just about 1% lower than those of the corresponding DI pastes. Additionally, compared with the hydration degree in C_3A-gypsum-SW pastes prepared without CH in Table 2, the presence of extra CH in the SW pastes also accelerated the hydration of C_3A in the later ages: the hydration degrees were increased by 4.5 % and 1.9 % at 96 h and 192 h, respectively. This specific role of CH on the later hydration of C_3A in SW pastes will be further discussed in Section 4.4.

Fig. 8 presents the hydration products at 96 h and 192 h for C_3A-gypsum-CH-DI/SW pastes prepared with a W/S ratio of 1. For C_3A-gypsum-CH-SW paste, there was a small amount of unreacted C_3A compared with the corresponding DI paste, especially at 96 h, which was consistent with QXRD result in Table 3. Besides, there was still no C_3AH_6 in SW paste due to the presence of too much chloride in seawater. Considering the comparable reaction sequence between C_3A-gypsum pastes and C_3A-gypsum-CH pastes, the thermodynamic modelling was not presented in this section.

Table 3. Hydration degree of C_3A in C_3A-gypsum-CH-DI/SW pastes with a W/S' ratio of 1 as calculated by QXRD.

Ages	C_3A+G+CH+DI	C_3A+G+CH +SW
30 h	10.8	26.1
40 h	11.6	35.2
96 h	97.3	96.2
192 h	98.4	97.6

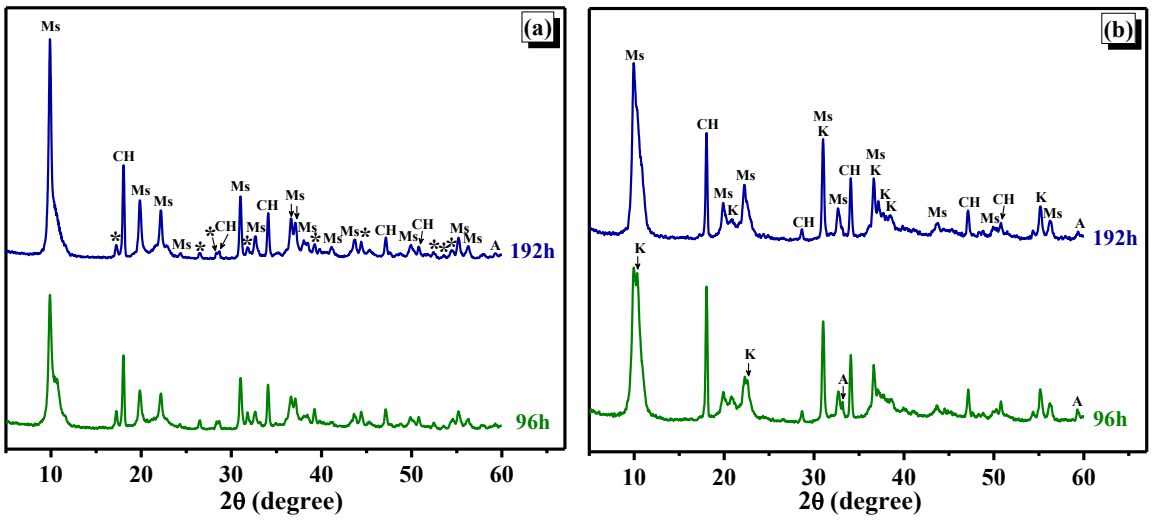

Fig. 8. Hydration products at 96 h and 192 h for C_3A-gypsum-CH-DI paste (a) and C_3A-gypsum-CH-SW paste (b) with a W/S ratio of 1. (A: C_3A (tricalcium aluminate), Ms: SO_4-AFm-12, K: Kuzel's salt, ✻: C_3AH_6 (hydrogarnet).)

4. Further discussion

4.1. Explanation on the reaction sequence in C_3A-gypsum-SW pastes

Referring to the calculated Gibbs free energies in Table 4, it was found that the precipitation of AFt has a lower Gibbs energy than the formation of Friedel's salt and Kuzel's salt, indicating that the former reaction is more favourable. It was consistent with the reported results that, when Cl^- and SO_4^{2-} were present simultaneously in the solution, C_3A was prone to preferentially bind with SO_4^{2-} to form AFt.[9, 56-58] Likewise, when seawater was used as the mixing water, the initial hydration product precipitated was AFt.

In addition, the Gibbs energies of precipitating of Friedel's salt, Kuzel's salt and SO_4-AFm were comparable, and it is difficult to determine which one was the preferred. Considering that they all belong to a same calcium-aluminium layered double hydroxide (Ca-Al LDH) family, there was a highest affinity for Cl^- to be attracted into the interlayer spaces of Ca-Al LDH, followed by SO_4^{2-} and OH^-.[59-61] Consequently, this could lead to the preferential formation of Friedel's salt and Kuzel's salt compared with SO_4-AFm in the seawater system (Fig. 5), and

OH^- was the last to enter the interlayer spaces of Ca-Al LDH to form OH-AFm and then converted into C_3AH_6.

Table 4. Gibbs free energies ($\Delta_r G^0$) of the precipitation process of AFt, Friedel's salt (Fs), Kuzel's salt (Ks) and SO_4-AFm.

Reaction	$\Delta_r G^0$(kJ/mol)
$6Ca^{2+}+2AlO_2^-+4OH^-+3SO_4^{2-}+30H_2O \rightarrow 3CaO\cdot Al_2O_3\cdot 3CaSO_4\cdot 32H_2O$ (AFt)	-256.38
$4Ca^{2+}+2AlO_2^-+4OH^-+2Cl^-+8H_2O \rightarrow 3CaO\cdot Al_2O_3\cdot CaCl_2\cdot 10H_2O$ (Fs)	-155.68
$4Ca^{2+}+2AlO_2^-+4OH^-+0.5SO_4^{2-}+Cl^-+10H_2O \rightarrow 3CaO\cdot Al_2O_3\cdot 0.5CaSO_4\cdot 0.5CaCl_2\cdot 12H_2O$ (Ks)	-162.88
$4Ca^{2+}+2AlO_2^-+4OH^-+SO_4^{2-}+10H_2O \rightarrow 3CaO\cdot Al_2O_3\cdot CaSO_4\cdot 12H_2O$ (SO_4-AFm)	-166.94

Note: $\Delta_f G^0$ information for the substances used in calculation is referenced in [40, 62].

4.2. Dissolution driving force of C_3A in DI and seawater systems

The ionic concentrations in pore solution (Figs. 3 and 7) can be used to calculate the saturation index (SI) of C_3A, and the result is shown in Fig. 9. It was observed that all SI values of C_3A at different reaction times were negative, indicating a process of continuous dissolution of C_3A with the hydration time. In comparison, the SI values of C_3A in SW system was lower than that in DI system, especially for early C_3A-gypsum system in Fig. 9 (a). This indicated that there was a large dissolution driving force of C_3A in seawater compared with that in DI water. The specific reasons can be attributed to lower pH value in the very early age (Fig. 3 (g)) and higher ionic strength of seawater (about 0.57 mol/L). The higher ionic strength of seawater can decrease the activity coefficient of solute ions, which would increase the concentration of ions (for example Ca^{2+} in Figs. 3 and 7) to maintain the solubility product constant of C_3A. This would lead to a larger dissolution of C_3A in seawater.

Besides, it was also found that, at later ages, the SI values of C_3A in C_3A-gypsum-SW system were slightly larger than that in C_3A-gypsum-DI system (Fig. 9 (a)). But, when CH was present in reaction system, there were a relatively lower SI values of C_3A in the C_3A-gypsum-CH-SW paste at 120 h and 168 h (Fig. 9 (b)). This would further illustrate that the accumulation of Al in the reaction solution of C_3A-gypsum-SW paste (Fig. 3) hindered the dissolution of C_3A at the later ages to a certain degree. When sufficient CH was supplied, the dissolution driving force of C_3A at the later ages increased correspondingly due to the disappear of accumulation of Al in the reaction solution (Fig. 7 (a)).

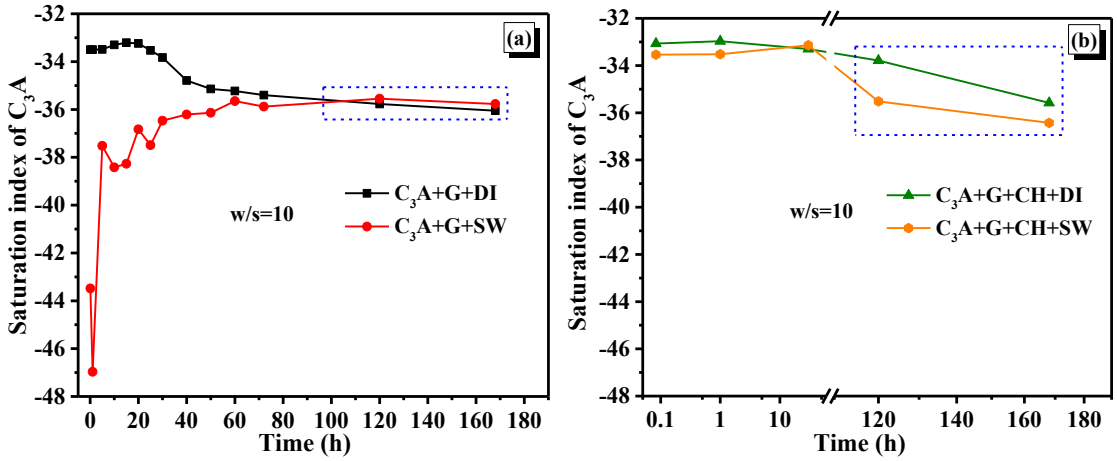

Fig. 9. Saturation index of C_3A in C_3A-gypsum-DI/SW system (a) and C_3A-gypsum-CH-DI/SW system (b) calculated as a function of hydration time. The negative number for saturation index denotes undersaturation sate.

4.3. Accelerating effect of seawater on early hydration of C_3A in C_3A-gypsum pastes

In both the C_3A-gypsum and C_3A-gypsum-CH reaction systems, it was found that seawater promoted the hydration degree of C_3A during the formation of AFt (Tables 2 and 3). The reasons could be ascribed to that: 1) seawater increased the dissolution driving force of C_3A as mentioned in the above section, 2) seawater also increased the solubility of gypsum, which will be explained in the following contents.

By comparing the initial concentration of SO_4^{2-} in different DI and SW solutions (Fig. 10) or in the extracted pore solution of the C_3A pastes (Fig. 3), it was found that the solubility of SO_4^{2-} in seawater was significantly higher than that in the DI water. Even though the solubility of SO_4^{2-} decreased in the saturated CH solution due to the common ion effect (i.e., Ca^{2+}), its concentration in the SW solutions was still higher than that in the corresponding DI solution (Fig. 10). This could be ascribed to that the stronger ionic interactions caused by the higher ionic strength of seawater can decrease the activity coefficients of Ca^{2+} and SO_4^{2-}. This would increase the concentrations of these two ions in order to maintain the solubility product constant of gypsum, which consequently led to a larger solubility of gypsum.[63, 64]

Thus, both the much more dissolution of C_3A (Fig. 9) and higher solubility of gypsum resulted in a greater supersaturation with respect to AFt, causing a relatively faster reaction between gypsum and C_3A to form AFt (Fig. 5). For this reason, there was a higher hydration degree of C_3A before the depletion of gypsum (Tables 2 and 3). This rapid precipitation of AFt in the SW paste compared with the DI paste could also explain why seawater can lead to fast setting and high loss of workability as reported in seawater mixed cement concrete from the perspective of C_3A hydration.[11, 12, 15-18]

After the formation of AFt, when comparing the residual concentration of SO_4^{2-} in the pore solution of SW and DI pastes (Figs. 3 (c) and 3 (f)), it was found that the concentration of remaining SO_4^{2-} in the SW paste was higher than that in the DI paste. This could also be due to the higher solubility of gypsum in seawater, in comparison to that in DI water. When the solid gypsum in the reaction system was completely dissolved, there would result in an undersaturated state of SO_4^{2-} in solution. This would cause a desorption of SO_4^{2-} from the surface of C_3A. Thus, in the seawater system with a larger solubility of gypsum, there would be a more residual SO_4^{2-} in solution to re-establish the dynamic equilibrium.

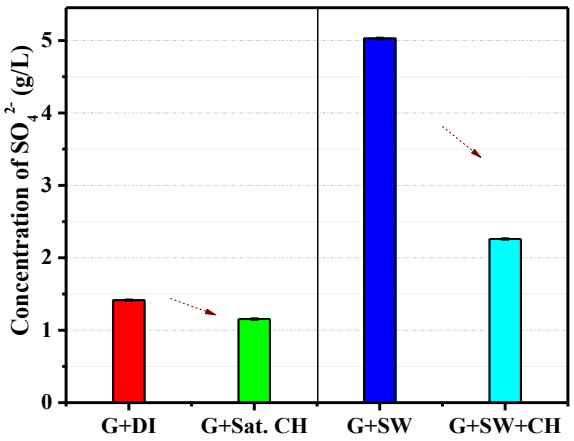

Fig. 10. Equilibrium concentration of SO_4^{2-} in different solutions. A sufficient amount of gypsum was added into DI water (G+DI), saturated CH solution (G+Sat. CH), SW (G+SW) and a mixture of SW and sufficient CH (G+SW+CH). Then, the supernatant was used to measure the concentration of SO_4^{2-}.

4.4. The role of Ca (element) in the later hydration process of C_3A-gypsum-SW pastes

As depicted in the schematic diagram in Fig. 11, when CH was absent in the reaction system, the Ca (element) dissolved from C_3A was completely consumed (Figs. 3 (b) and 3 (e)) in the period of forming Friedel's salt and Kuzel's salt, and consequently there was an accumulation of Al (element) (Figs. 3 (a) and 3 (d)) and OH^- in the solution. Thus, this resulted in a slower dissolution rate of C_3A (Fig. 9 (a) & wider exothermic peak in Fig. 2 (a)) and an increase of pH (Fig. 3 (g)) at later ages. The same phenomenon was also found in the C_3A-SW system prepared without gypsum in our previous study.[22] In comparison, when sufficient CH was provided for the formation of Friedel's salt and Kuzel's salt in the C_3A-gypsum-CH-SW paste, there was no accumulation of Al during this reaction process (Fig. 7 (a)). But the consumption of Ca derived from CH in this reaction would release OH^- to increase the pH value of the pore solution (Fig. 7 (d)). Furthermore, this higher undersaturated Al with respect to C_3A would markedly increase the dissolution rate of the subsequent C_3A (Fig. 2 (a) vs. Fig. 6 (a)), leading

to an increase of hydration degree of C_3A at 96 h and 192 h (Table 2 vs. Table 3), in comparison to that of the C_3A-gypsum-SW paste.

However, even though a sufficient CH was present, there was still a slightly broader main exothermic peak and marginally lower hydration degree in the C_3A-gypsum-CH paste at the later ages compared with the corresponding DI paste. This could be due to that the precipitation of Mg on the C_3A surface at initial hydration (Fig. 3 (b)) which blocked some active sites available for further C_3A hydration. This has also been pointed out in our previous study.[22] As mentioned in Section 4.3, when gypsum was exhausted due to the formation of AFt, the depletion of SO_4^{2-} in the pore solution would result in a net desorption of SO_4^{2-} from the C_3A surface, leading to the end of the induction period and the beginning of acceleration period.[47, 65] However, the attachment of magnesium product on C_3A surface in the SW paste did not desorb like SO_4^{2-}, which could marginally reduce the dissolution rate of C_3A due to the reduced exposure to water.

Based on the above analysis, the hydration process of C_3A pastes mixed with seawater was strongly dependent on the amount of Ca available in the reaction system and partly dependent to the precipitation of magnesium product on C_3A surface, especially after the consumption of gypsum. The role of Ca may be further extended to other cementitious environments: 1) if seawater is used to prepare a cementitious material through incorporating ≥ 40 % pozzolans and other SCMs,[66-68] the low Ca in this system may obviously retard the hydration of C_3A in the period after the depletion of gypsum, further inhibiting the formation of C_3AH_6 at the later age. 2) if seawater is used in the conventional OPC cement concrete, the portlandite hydrated from C_3S or C_2S would provide sufficient Ca for the formation of Friedel's salt and Kuzel's salt. The retardation effect of seawater on the hydration of C_3A derived from the deficiency of Ca and accumulation of Al would be mitigated to some degrees. On the contrary, the forming process of Friedel's salt or Kuzel's salt would need to consume more portlandite compared

with the DI pastes, which could also accelerate the hydration of C_3S or C_2S in the cement to a certain extent.

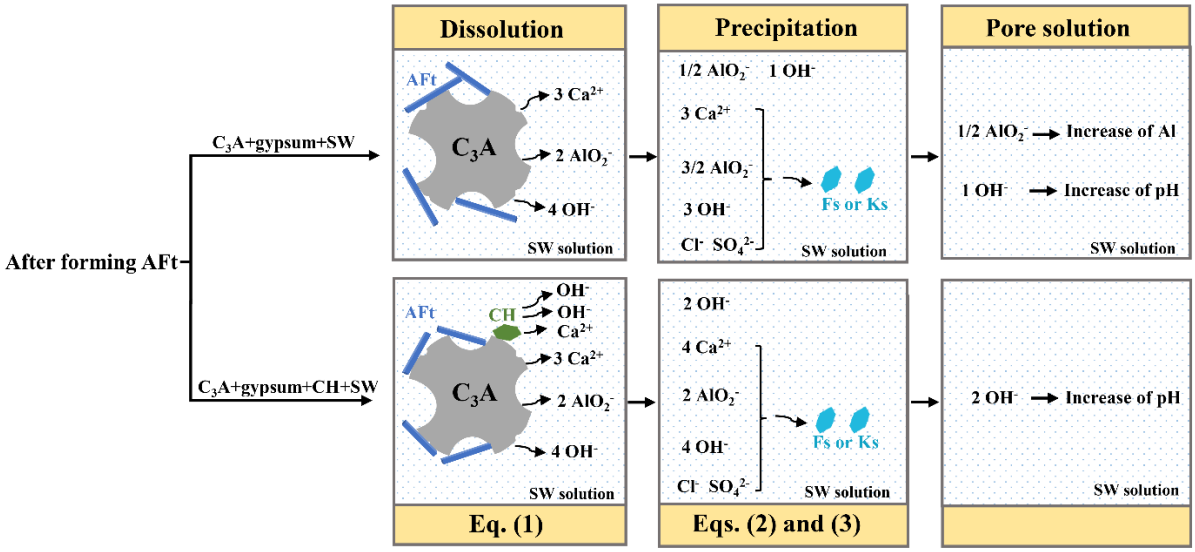

(1) $Ca_3Al_2O_6(C_3A)+2\ H_2O \rightarrow 3\ Ca^{2+}+2\ AlO_2^-+4\ OH^-$

(2) $4Ca^{2+}+2\ AlO_2^-+2Cl^-+4\ OH^-+8H_2O \rightarrow Ca_4Al_2Cl_2(OH)_{12}\cdot 4H_2O\ (Fs)$

(3) $4Ca^{2+}+2AlO_2^-+4OH^-+0.5SO_4^{2-}+Cl^-+10H_2O \rightarrow 3CaO\cdot Al_2O_3\cdot 0.5CaSO_4\cdot 0.5CaCl_2\cdot 12H_2O\ (Ks)$

Fig. 11. Schematic diagram of ionic changes in the process of the dissolution of C_3A and the precipitation of Friedel's salt and Kuzel's salt after the formation of AFt.

5. Conclusions

The purpose of this work was to elucidate how seawater affected the hydration process of the C_3A in C_3A-gypsum and C_3A-gypsum-CH reaction systems. The evolution of hydration heat, ionic concentration in the pore solution and hydration products were investigated by isothermal calorimetry, ICP-OES, Ion Chromatography, XRD and thermodynamic modelling. The main findings are as follows:

- Seawater accelerated the early hydration of C_3A and the formation of AFt in both the C_3A-gypsum and C_3A-gypsum-CH reaction systems, leading to a higher hydration degree of

C_3A at the early age compared with DI pastes. This is mainly attributed to a larger dissolution driving force of C_3A and higher solubility of gypsum in seawater.

- The Ca available in SW pastes played a dominant role in controlling the hydration rate of C_3A after the depletion of gypsum. When there was no extra Ca in the C_3A-gypsum system, the accumulation of Al due to the lack of Ca during the formation of Friedel's salt and Kuzel's salt would slow down the dissolution rate of the remaining C_3A, which would reduce the dissolution driving force of C_3A at later ages to further decrease the hydration degree of C_3A. However, when extra CH was present in the C_3A-gypsum system, the sufficient Ca source did not cause the accumulation of Al in the pore solution. Meanwhile, the hydration degree of C_3A in this case increased as well, compared with that of the C_3A-gypsum-SW paste.
- When CH was absent in the system, the slower dissolution rate of C_3A at the later ages resulted in the slower formation of Kuzel's salt and the slower transformation of AFt to SO_4-AFm. This would further retard the formation of C_3AH_6 in the C_3A-gypsum-SW paste compared to the corresponding DI paste.

Acknowledgments

The authors would like to acknowledge the financial support by the Research Grants Council of the Hong Kong SAR Government (Project No. T22-502/18-R), Lantau Conservation Fund (Project No. RE-2020-08) and The Hong Kong Polytechnic University. Besides, the authors would like to thank Dr. Xiaohong Zhu for his help with the calculation of saturation index and Prof. Barbara Lothenbach for helpful discussion on the thermodynamic analysis.

Reference

1. Mindess S. Sustainability of concrete. Developments in the Formulation and Reinforcement of Concrete. Woodhead Publishing; 2019;3-17.
2. Naik TR. Sustainability of the cement and concrete industries. Proceedings of the International Conference on Achieving Sustainability in Construction; 2007.
3. Im S, Jee H, Suh H, Kanematsu M, Morooka S, Taku K, Yuhei N, Machida A, Kim J, Bae S. Temperature effects on local structure, phase transformation, and mechanical properties of calcium silicate hydrates. J Am Ceram Soc. 2021;104:4803-18.
4. https://www.statista.com/study/102356/global-cement-industry/.
5. https://www.statista.com/statistics/373845/global-cement-production-forecast/.
6. Miller SA, Horvath A, Monteiro PJM. Impacts of booming concrete production on water resources worldwide. Nat Sustain. 2018;1:69-76.
7. Guo F, Al-Saadi S, Raman RS, Zhao X. Durability of fiber reinforced polymer (FRP) in simulated seawater sea sand concrete (SWSSC) environment. Corros Sci. 2018;141:1-13.
8. Wang Z, Zhao X-L, Xian G, Wu G, Raman RS, Al-Saadi S, Haque A. Long-term durability of basalt- and glass-fibre reinforced polymer (BFRP/GFRP) bars in seawater and sea sand concrete environment. Constru Build Mater. 2017;139:467-89.
9. Li P, Li W, Yu T, Qu F, Tam VWY. Investigation on early-age hydration, mechanical properties and microstructure of seawater sea sand cement mortar. Constru Build Mater. 2020;249:118776
10. Guo M, Hu B, Xing F, Zhou X, Sun M, Sui L, Zhou Y. Characterization of the mechanical properties of eco-friendly concrete made with untreated sea sand and seawater based on statistical analysis. Constru Build Mater. 2020;234:117339.
11. Younis A, Ebead U, Suraneni P, Nanni A. Fresh and hardened properties of seawater-mixed concrete. Constru Build Mater. 2018;190:276-86.
12. Sikora P, Cendrowski K, Abd Elrahman M, Chung S-Y, Mijowska E, Stephan D. The effects of seawater on the hydration, microstructure and strength development of Portland cement pastes incorporating colloidal silica. Appl Nanosci. 2019;10:2627-38.
13. Wang J, Liu E, Li L. Multiscale investigations on hydration mechanisms in seawater OPC paste. Constru Build Mater. 2018;191:891-903.
14. Li W, Jiang Z, Lu M, Long W, Xing F, Liu J. Effects of seawater, NaCl, and Na_2SO_4 solution mixing on hydration process of cement paste. J Mater Civ Eng. 2021;33:04021057.
15. Ghorab HY, Hilal M, Antar AJC. Effect of mixing and curing waters on the behaviour of cement pastes and concrete Part 2: Properties of cement paste and concrete. Cem Concr Res. 1990;20:69-72.
16. Etxeberria M, Gonzalez-Corominas A, Pardo P. Influence of seawater and blast furnace cement employment on recycled aggregate concretes' properties. Constru Build Mater. 2016;115:496-505.
17. Li L, Chen X, Chu S, Ouyang Y, Kwan A. Seawater cement paste: effects of seawater and roles of water film thickness and superplasticizer dosage. Constru Build Mater. 2019;229:116862.

18. Hussain Z, Noor NM, Caronge MA. Workability and Compressive Strength of Seawater-Mixed Concrete Containing Rice Husk Ash as Supplementary Cementitious Material. Int J Integr Eng. 2019;11:192-200.
19. Hou P, Wang X, Zhao P, Wang K, Kawashima S, Li Q, Xie N, Cheng X, Shah SP. Physicochemical effects of nanosilica on C_3A/C_3S hydration. J Am Ceram Soc. 2020;103:6505-18.
20. Hirsch T, Lu Z, Stephan D. Impact of triethanolamine on the sulfate balance of Portland cements with mixed sulfate carriers. J Am Ceram Soc. 2021;104:4829-42.
21. Quennoz A, Scrivener KL. Interactions between alite and C_3A-gypsum hydrations in model cements. Cem Concr Res. 2013;44:46-54.
22. Cai Y, Xuan D, Hou P, Shi J, Poon CS. Effect of seawater as mixing water on the hydration behaviour of tricalcium aluminate. Cem Concr Res. 2021;149:106565.
23. Ramachandran VS. Differential thermal method of estimating calcium hydroxide in calcium silicate and cement pastes. Cem Concr Res. 1979;9:677-84.
24. Taylor H, Newbury D. Calcium hydroxide distribution and calcium silicate hydrate composition in tricalcium silicate and β-dicalcium silicate pastes. Cem Concr Res. 1984;14:93-98.
25. Cook R, Ma H, Okoronkwo M, Sant G, Kumar A. Influence of water activity on belite (β-C_2S) hydration. J Am Ceram Soc. 2021;104:1831-40.
26. Standard A. D1141-98: Standard Practice for the Preparation of Substitute Ocean Water. ASTM International, West Conshohocken. 2013.
27. Traetteberg A, GRATTAN-BELLEW PE. Hydration of $3CaO{\cdot}Al_2O_3$ and $3CaO{\cdot}Al_2O_3$+Gypsum With and Without $CaCl_2$. J Am Ceram Soc. 1975;58:221-27.
28. Ramírez A, Pauli J, Mota B, Casselt C, Simon S, Schmidt W, Resch-Genger U. C_3A passivation with gypsum and hemihydrate monitored by optical spectroscopy. Cem Concr Res. 2020;133:106082.
29. Scrivener K, Snellings R, Lothenbach B. A practical guide to microstructural analysis of cementitious materials. Crc Press. 2018;48-49.
30. Maach N, Georgin J, Berger S, Pommay J. Chemical mechanisms and kinetic modeling of calcium aluminate cements hydration in diluted systems: Role of aluminium hydroxide formation. Cem Concr Res. 2021;143:106380.
31. Mondal P, Jeffery J. The crystal structure of tricalcium aluminate, $Ca_3Al_2O_6$. Acta Crystallogr B. 1975;31:689-97.
32. Boeyens J, Ichharam V. Redetermination of the crystal structure of calcium sulphate dihydrate, $CaSO_4{\cdot}2H_2O$. Zeitschrift für Kristallographie-new crystal structures. 2002;217:9-10.
33. Goetz-Neunhoeffer F, Neubauer. Refined ettringite ($Ca_6Al_2(SO_4)_3(OH)_{12}{\cdot}26H_2O$) structure for quantitative X-ray diffraction analysis. Powder Diffr. 2006;21:4-11.
34. Allmann R. Refinement of the hybrid layer structure $(Ca_2Al(OH)_6)^{+}{\cdot}(1/2SO_4{\cdot}3H_2O)^{-}$. 1977;

35. Lager GA, Downs RT, Origlieri M, Garoutte R. High-pressure single-crystal X-ray diffraction study of katoite hydrogarnet: Evidence for a phase transition from Ia3d→ $I\bar{4}3d$ symmetry at 5 GPa. Am Mineral. 2002;87:642-47.
36. Mesbah A, François M, Cau-dit-Coumes C, Frizon F, Filinchuk Y, Leroux F, Ravaux J, Renaudin G. Crystal structure of Kuzel's salt $3CaO{\cdot}Al_2O_3{\cdot}1/2CaSO_4{\cdot}1/2CaCl_2{\cdot}11H_2O$ determined by synchrotron powder diffraction. Cem Concr Res. 2011;41:504-09.
37. Chaix-Pluchery O, Pannetier J, Bouillot J, Niepce J. Structural prereactional transformations in Ca $(OH)_2$. J Solid State Chem. 1987;67:225-34.
38. Riello P, Canton P, Fagherazzi G. Calibration of the monochromator bandpass function for the X-ray Rietveld analysis. Powder Diffr. 1997;12:160-66.
39. Hummel W, Berner U, Curti E, Pearson F, Thoenen T. Nagra/PSI chemical thermodynamic data base 01/01. Radiochim Acta. 2002;90:805-13.
40. Lothenbach B, Kulik DA, Matschei T, Balonis M, Baquerizo L, Dilnesa B, Miron GD, Myers RJ. Cemdata18: A chemical thermodynamic database for hydrated Portland cements and alkali-activated materials. Cem Concr Res. 2019;115:472-506.
41. Lothenbach B, Le Saout G, Gallucci E, Scrivener K. Influence of limestone on the hydration of Portland cements. Cem Concr Res. 2008;38:848-60.
42. Lothenbach B, Matschei T, Möschner G, Glasser FP. Thermodynamic modelling of the effect of temperature on the hydration and porosity of Portland cement. Cem Concr Res. 2008;38:1-18.
43. Chaunsali P, Mondal P. Physico-chemical interaction between mineral admixtures and OPC–calcium sulfoaluminate (CSA) cements and its influence on early-age expansion. Cem Concr Res. 2016;80:10-20.
44. Hirao H, Yamada K, Takahashi H, Zibara H. Chloride binding of cement estimated by binding isotherms of hydrates. J Adv Concr Technol. 2005;3:77-84.
45. Sun Y, Zhang Y, Cai Y, Lam WL, Lu J-X, Shen P, Poon CS. Mechanisms on accelerating hydration of alite mixed with inorganic salts in seawater and characteristics of hydration products. ACS Sustain Chem Eng. 2021;9:10479-90.
46. Pourchet S, Regnaud L, Perez JP, Nonat A. Early C_3A hydration in the presence of different kinds of calcium sulfate. Cem Concr Res. 2009;39:989-96.
47. Minard H, Garrault S, Regnaud L, Nonat A. Mechanisms and parameters controlling the tricalcium aluminate reactivity in the presence of gypsum. Cem Concr Res. 2007;37:1418-26.
48. Quennoz A, Scrivener KL. Hydration of C_3A–gypsum systems. Cem Concr Res. 2012;42:1032-41.
49. Stein H. Some characteristics of the hydration of $3CaO{\cdot}Al_2O_3$ in the presence of $CaSO_4{\cdot}2H_2O$. Recueil des Travaux Chimiques des Pays-Bas. 1962;81:881-89.
50. Liu X, Feng P, Lyu C, Ye S. The role of sulfate ions in tricalcium aluminate hydration: New insights. Cem Concr Res. 2020;130:105973.

51. Joseph S, Skibsted J,Cizer Ö. A quantitative study of the C_3A hydration. Cem Concr Res. 2019;115:145-59.
52. Feldman R, Ramachandran VS. The influence of $CaSO_4 \cdot 2H_2O$ upon the hydration character of $3CaO \cdot Al_2O_3$. Mag. Concr. Res. 1966;18:185-96.
53. Mehta PK. Effect of lime on hydration of pastes containing gypsum and calcium aluminates or calcium sulfoaluminate. J Am Ceram Soc. 1973;56:315-19.
54. Taylor HF. Cement chemistry. Thomas Telford London, 1997;182-86.
55. Collepardi M, Baldini G, Pauri M, Corradi M. Tricalcium aluminate hydration in the presence of lime, gypsum or sodium sulfate. Cem Concr Res. 1978;8:571-80.
56. Hussain SE, Al-Gahtani AS. Influence of sulfates on chloride binding in cements. Cem Concr Res. 1994;24:8-24.
57. Ahmed DA, Mohammed MR. Influence of chloride ion on the hydration reaction of C_3A in presence of gypsum and lime. Adv Cem Res. 2011;23:309-16.
58. Cao Y, Guo L, Chen B, Wu J. Effect of pre-introduced sodium chloride on cement hydration process. Adv Cem Res. 2021;1-14.
59. Sudare T, Dubois M, Louvain N, Kiyama M, Hayashi F, Teshima K. Favorable intercalation of nitrate ions with fluorine-substituted layered double hydroxides. Inorg Chem. 2019;59:1602-10.
60. Puerta-Falla G, Balonis M, Falzone G, Bauchy M, Neithalath N, Sant GJI. Monovalent ion exchange kinetics of hydrated calcium-alumino layered double hydroxides. Ind Eng Chem Res. 2017;56:63-74.
61. Appelo C. The anion exchange properties of AFm (hydrocalumite-group) minerals defined from solubility experiments and crystallographic information. Cem Concr Res. 2021;140:106270.
62. Haynes WM. CRC handbook of chemistry and physics. CRC press, 2014.
63. Vogel AI, Jeffery GH. Vogel's textbook of quantitative chemical analysis. Wiley, 1989.
64. Dai Z, Kan AT, Shi W, Zhang N, Zhang F, Yan F, Bhandari N, Zhang Z, Liu Y, Ruan G. Solubility measurements and predictions of gypsum, anhydrite, and calcite over wide ranges of temperature, pressure, and ionic strength with mixed electrolytes. Rock Mech Rock Eng. 2017;50:327-39.
65. Bullard JW, Jennings HM, Livingston RA, Nonat A, Scherer GW, Schweitzer JS, Scrivener KL, Thomas JJ. Mechanisms of cement hydration. Cem Concr Res. 2011;41:1208-23.
66. Codina M, Cau-dit-Coumes C, Le Bescop P, Verdier J, Ollivier J. Design and characterization of low-heat and low-alkalinity cements. Cem Concr Res. 2008;38:437-48.
67. Zhang T, Cheeseman C, Vandeperre L. Development of low pH cement systems forming magnesium silicate hydrate (MSH). Cem Concr Res. 2011;41:439-42.
68. Bach T, Chabas E, Pochard I, Coumes CCD, Haas J, Frizon F, Nonat A. Retention of alkali ions by hydrated low-pH cements: Mechanism and Na^+/K^+ selectivity. Cem Concr Res. 2013;51:14-21.